Supplementary Information

Anisotropic ductility and thermoelectricity of van der Waals GeAs

Xia Jiang,[a,b] Tianqi Zhao,[c] and Dong Wang*[,a,b]

[a]Laboratory of Flexible Electronics Technology, Tsinghua University, Beijing 100084, P. R. China

[b]MOE Key Laboratory of Organic OptoElectronics and Molecular Engineering, Department of Chemistry, Tsinghua University, Beijing 100084, P. R. China

[c]AI for Science Institute, Beijing, 100080, P. R. China

*Corresponding author. orcid.org/0000-0002-0594-0515; Email: dong913@tsinghua.edu.cn

Supplementary Methods

Electrical Transport Coefficients Calculation. The coarse **k**-mesh used to determine MLWFs was 6×6×6 for GeAs. This means that the crystal we computed is a Wigner-Seitz cell corresponding to a 6×6×6 supercell built on the primitive cell. In such a Wigner-Seitz cell, the maximum hopping distance for MLWFs can be up to 23 Å. The hopping terms of the Hamiltonian in the Wannier representation with the hopping distance outside the Wigner-Seitz cell will be truncated in the Wannier interpolation. More detailed information can be found in Ref. [1]. As shown in Figure S3a, the Hamiltonian in the Wannier representation (||H(R)||) decays exponentially with the increasing hopping distance, R. Especially, when R = 23 Å the ratio of ||H(23 Å)|| to ||H(0)|| has decreased to 2.8×10^{-4}. The error in constructing the electron Hamiltonian for an arbitrary **k**-point introduced by the Wannier interpolation will be less than 0.1%.[2] On the other hand, the dynamical matrix in the Wannier representation is proportional to the interatomic force constants, whose spatial decay (Figure S3b) exhibits similar behavior as that for ||H(R)||. Therefore, the electron Hamiltonian and phonon dynamical matrix in the Wannier representation constructed on the 6×6×6 coarse **k**-mesh and **q**-mesh are sufficient to interpolate the electron-phonon coupling properties. To validate the accuracy of the interpolation, we depicted the electronic band structure and phonon dispersion along the high symmetry lines obtained with DFT calculation and Wannier interpolation, respectively, in Figure S3c and Figure S3d. The agreement is satisfactory.

The calculation of thermoelectric transport coefficients involves integration on an extremely dense **k**-mesh or **q**-mesh in the Brillouin zone (BZ). The higher the sampling density, the more accurate the integration. However, considering the computational cost, it is impossible to sample infinite grids. To get the convergence test of electrical transport coefficients, we used 40×40×32 and 50×50×42 fine **k**-meshes to sample the BZ and calculated the conductivity, as shown in Figure S4. We can see that the conductivity has basically converged on the **k**-mesh of 50×50×42. While the conductivity along the $[1\bar{1}0]$ direction shows small variations when the Fermi level shifts significantly into the VB or CB, these deviations are not relevant to the thermoelectric properties at the optimal doping level.

Lattice Thermal Conductivity Calculation. To obtain third-order IFCs, a 3×3×2 supercell containing 216 atoms was constructed, and only Γ-point was used in the self-consistent calculation. A cut-off radius of 6.5 Å was introduced to account for only interactions within this distance based on the convergence test of κ_l. The BTE can be solved either iteratively or in the relaxation time approximation (RTA) which treats Normal scattering processes as resistive. The computational cost of the former is much higher. To tackle this problem, we first examined the processes of phonon–phonon scattering using a moderate **q**-mesh. The three-phonon scattering processes can be decomposed into Normal/Umklapp processes or absorption/emission processes.[3] The frequency dependent phonon scattering rates were compared in Figure S5a. The scattering rate of the U process is comparable to the total scattering rate, especially for low-frequency phonons, implying that the phonon–phonon scattering is dominated by the U process. As such, the thermal conductivity based on the RTA should be sufficiently accurate, with < 3% deviation from the iterative solution on the moderate **q**-mesh. The convergence test of lattice thermal conductivity in the RTA with respect to the sampling density in the BZ was depicted in Figure S5b. Ultimately, the **q**-mesh of 30×30×30 was chosen for the integration in the BZ.

Supplementary Figures

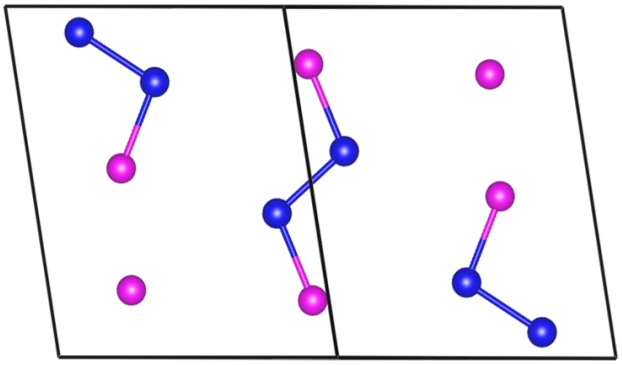

Figure S1. Primitive cell of GeAs with six Ge (blue) and six As (purple) atoms in it.

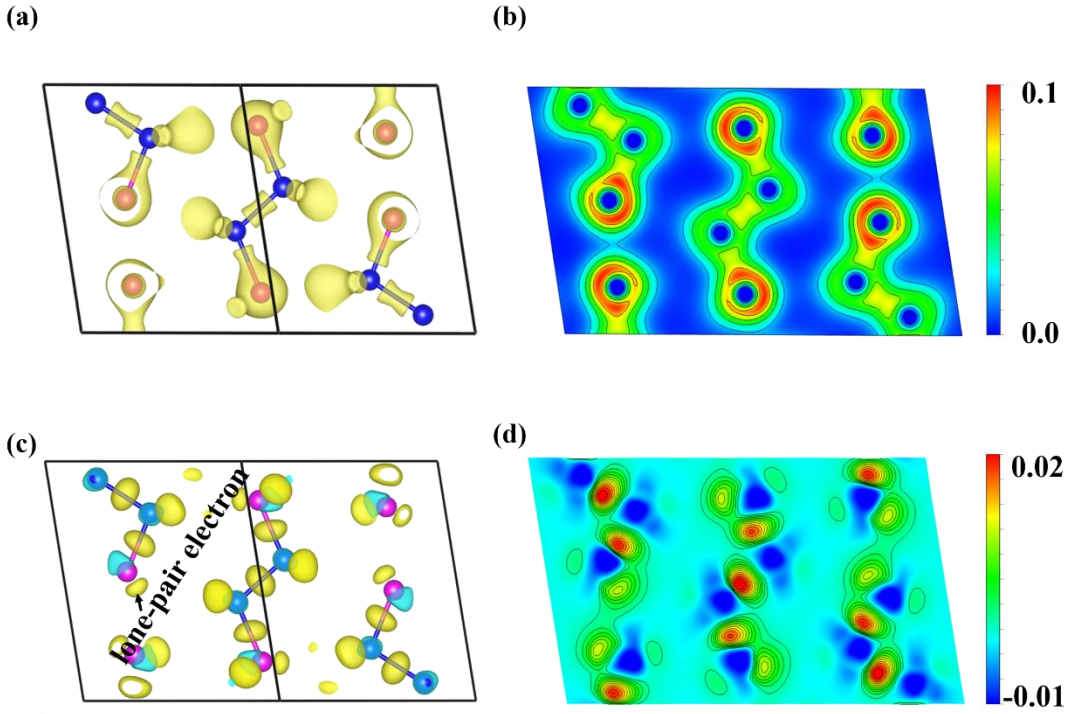

Figure S2. (a) Charge density distribution (isosurface value is 0.06 Bohr^{-3}) of GeAs. (b) Charge density distribution projected onto the $(1\bar{1}0)$ crystal plane. (c) Differential charge density (isosurface value is 0.008 Bohr^{-3}). The yellow and blue regions represent gaining and losing electrons, respectively. (d) Differential charge density projected onto the $(1\bar{1}0)$ crystal plane.

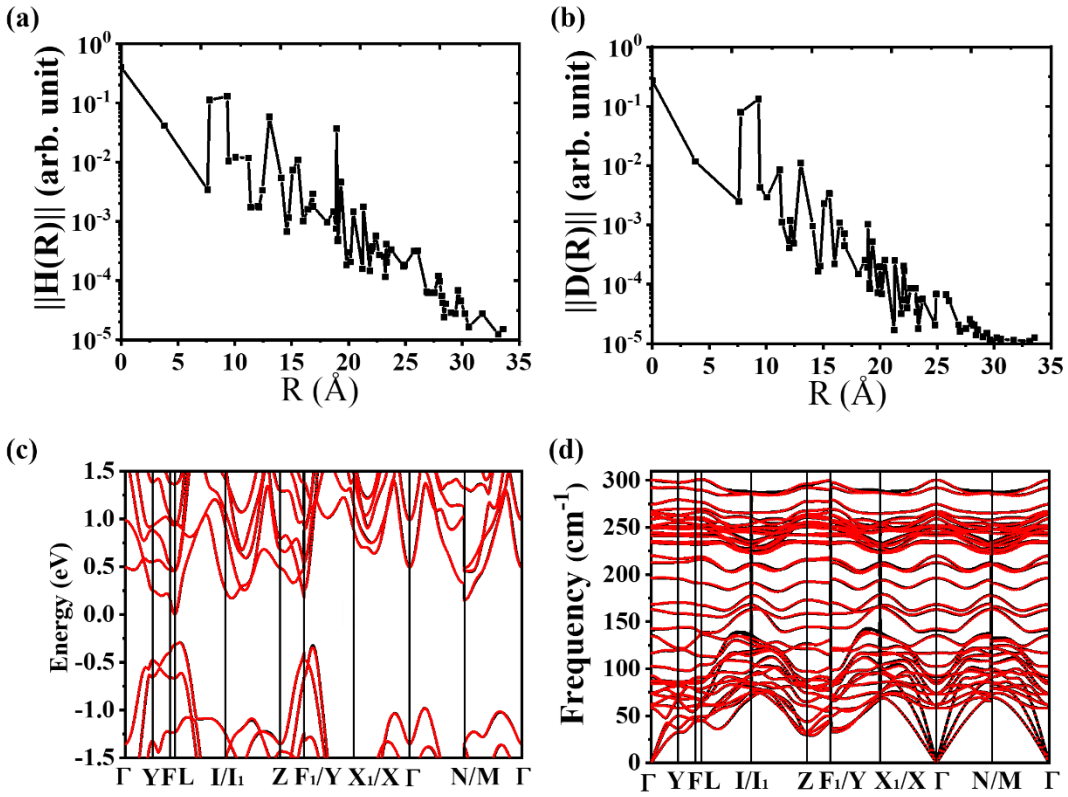

Figure S3. Spatial decay of (a) electron Hamiltonian and (b) dynamical matrix in the Wannier representation. Comparison of (c) band structures and (d) phonon spectra between DFT calculations (black solid lines) and Wannier-interpolations on the 6×6×6 coarse **k**-mesh and **q**-mesh, respectively (red dotted lines).

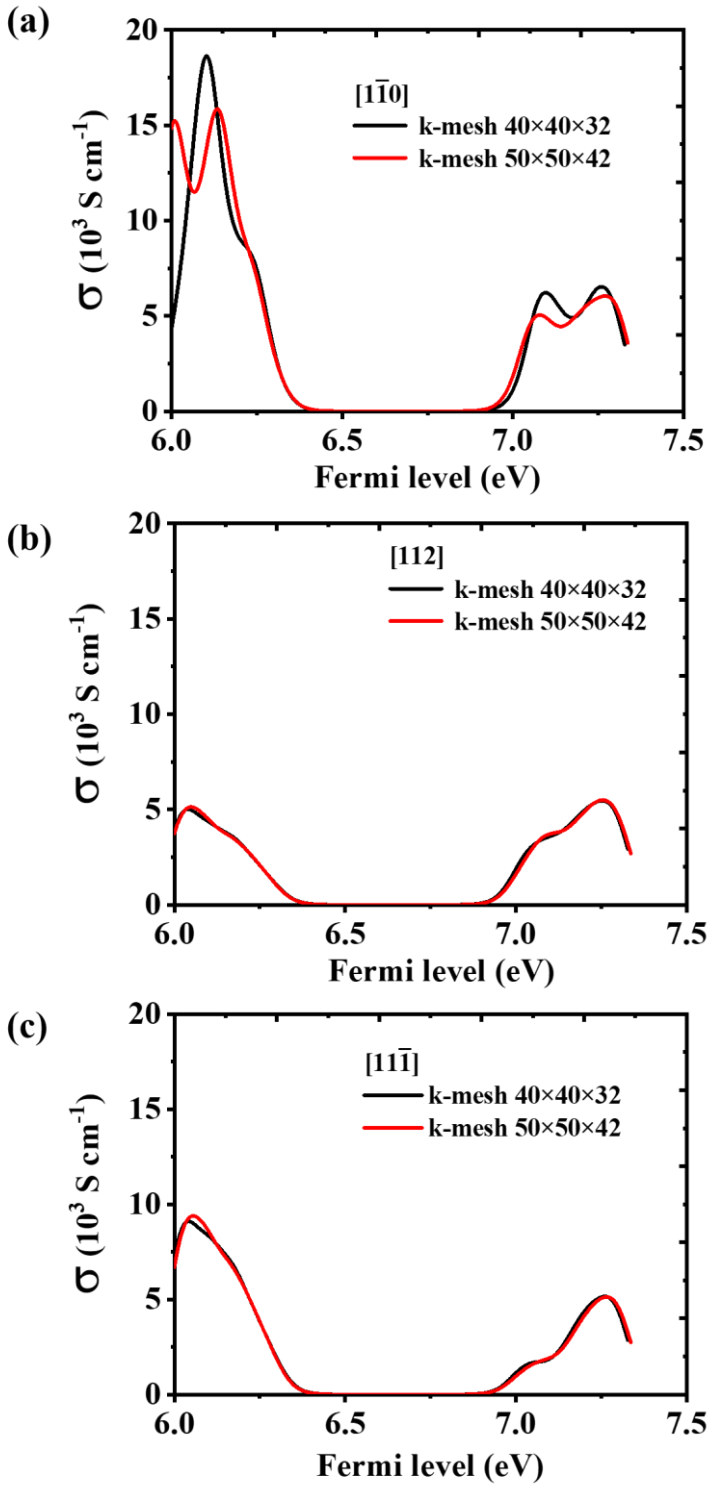

Figure S4. Electrical conductivity (σ) as a function of the Fermi level in the (a) [1$\bar{1}$0], (b) [112], and (c) [11$\bar{1}$] directions, obtained by integration over 40×40×32 and 50×50×42 fine **k**-meshes, respectively.

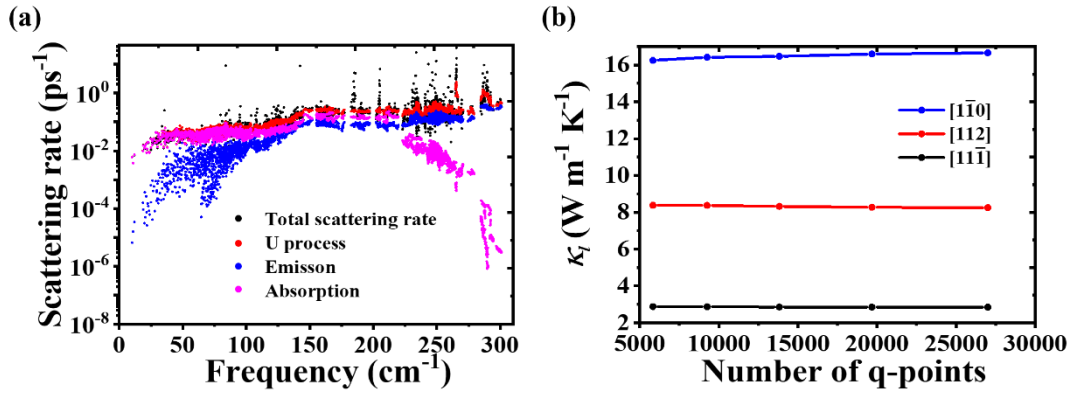

Figure S5. (a) Total scattering rate due to both Umklapp (U) and Normal (N) scattering processes and that due to the U scattering alone. The three-phonon scattering processes are also decomposed into phonon absorption and phonon emission processes. (b) Lattice thermal conductivities in the [1$\bar{1}$0], [112], and [11$\bar{1}$] directions, respectively, calculated by integration over different numbers of **q**-points sampled in the Brillouin zone.

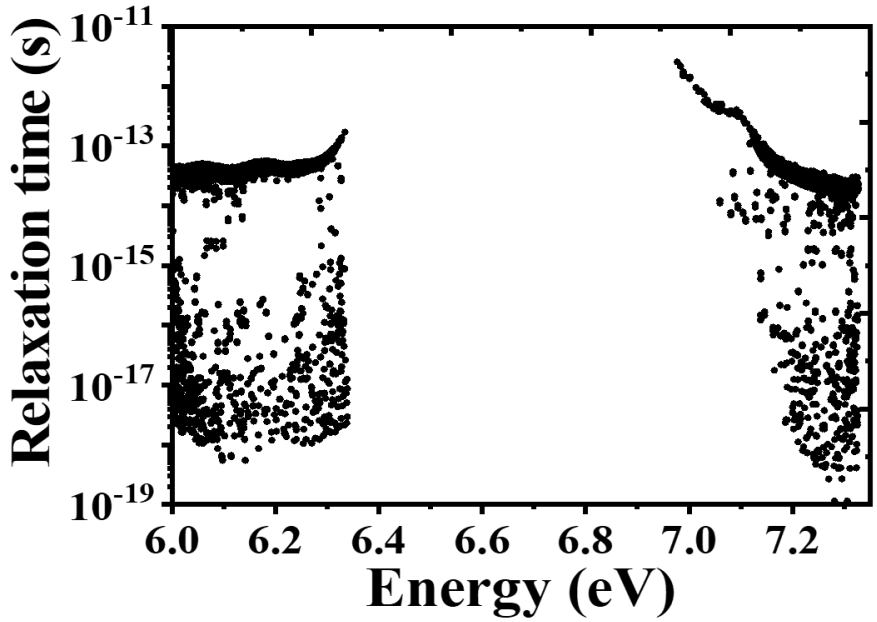

Figure S6. Relaxation times of electrons and holes as a function of the energy of charge carriers.

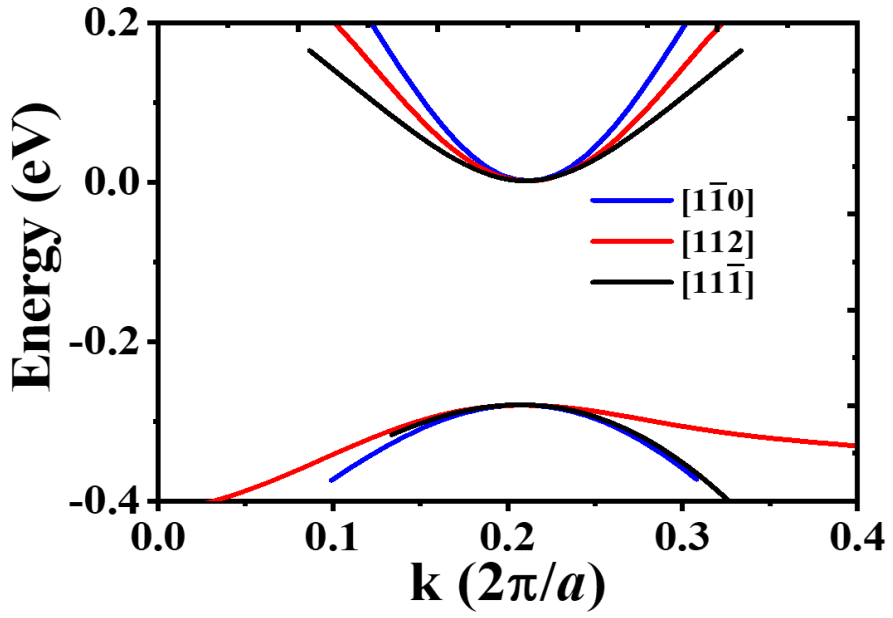

Figure S7. Band dispersion relations around the VBM and CBM along the [1$\bar{1}$0], [112], and [11$\bar{1}$] directions, respectively, for the effective mass calculation. *a* is the lattice constant in the [100] direction.

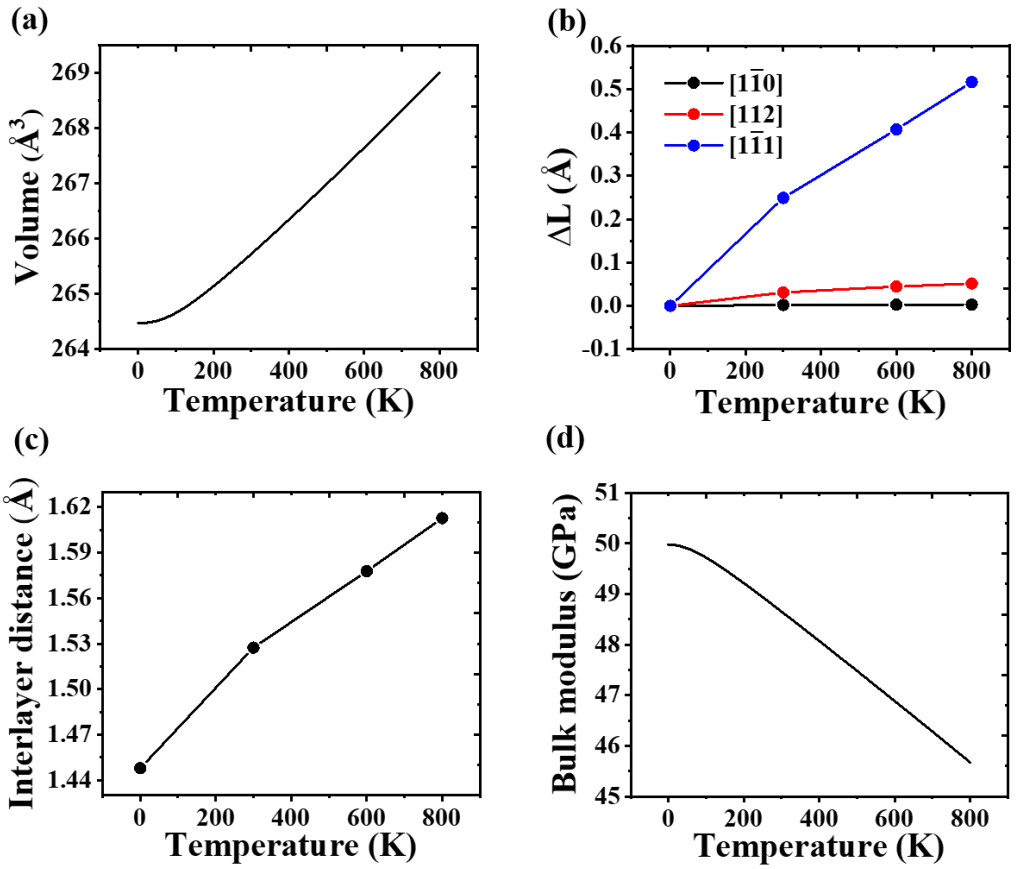

Figure S8. (a) Crystal volume, (b) lattice parameters, (c) interlayer distance, and (d) isothermal bulk modulus changing with temperature.

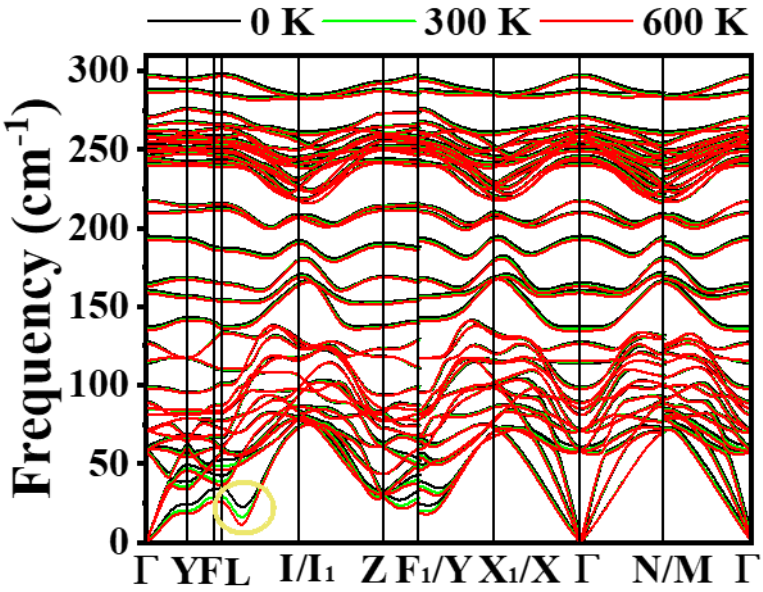

Figure S9. Phonon spectra at 0 K, 300 K, and 600 K, respectively.

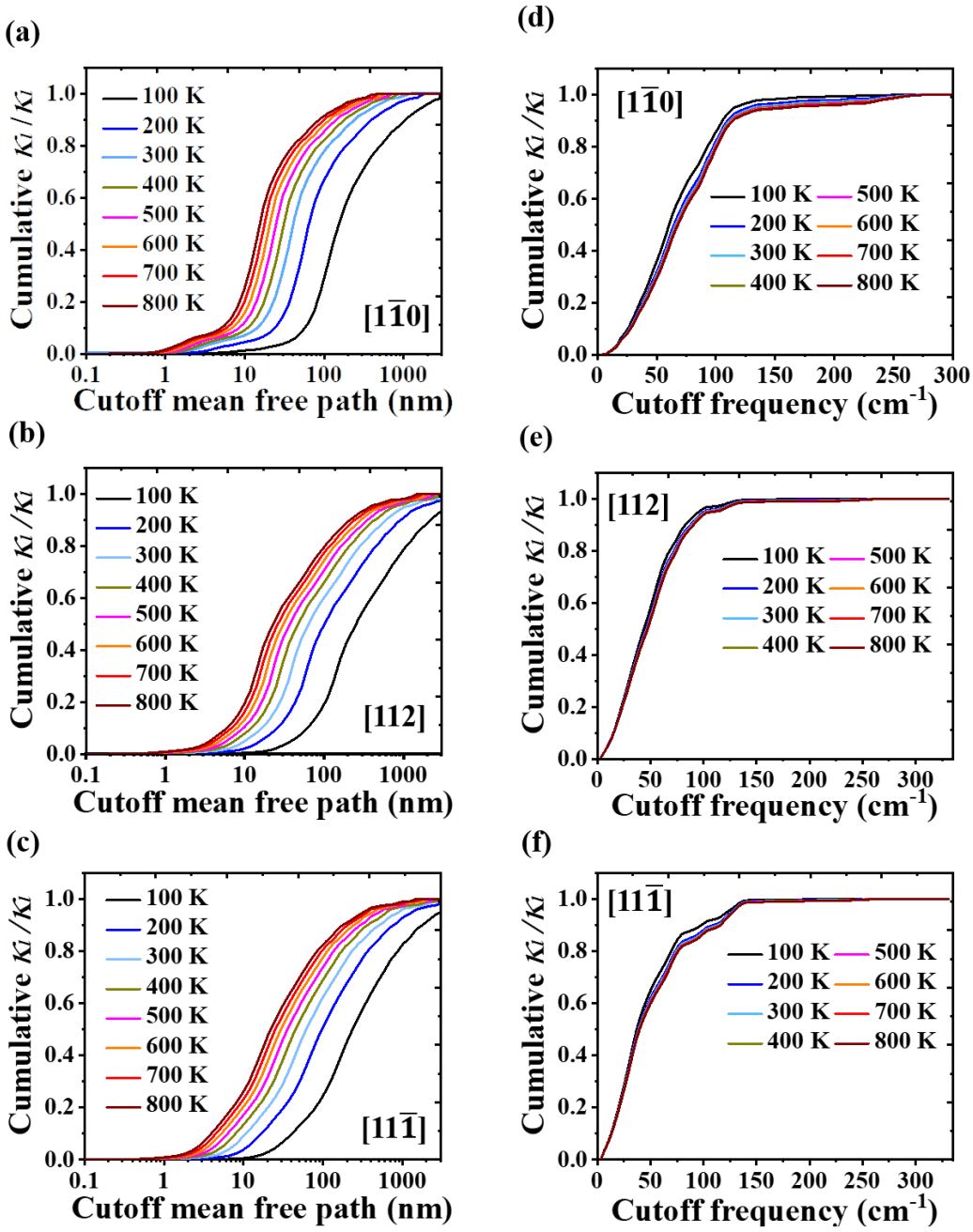

Figure S10. (a-c) Cumulative lattice thermal conductivity along the [1$\bar{1}$0], [112], and [11$\bar{1}$] directions, respectively, changing with the cut-off frequency of phonons. The temperature ranges from 100 K to 800 K. (d-f) Cumulative lattice thermal conductivity changing with the cut-off mean free path of phonons.

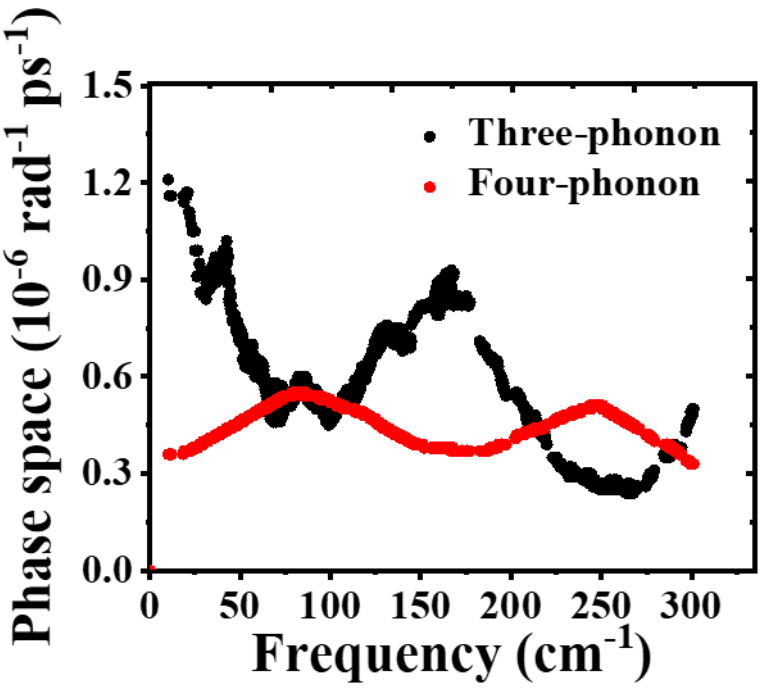

Figure S11. Phase space of three-phonon and four-phonon scatterings changing with the frequency of phonons.

Supplementary Tables

Table S1. The high-symmetry points in the first Brillouin zone used for band structure and phonon spectra calculations. $\mathbf{b}_1$, $\mathbf{b}_2$, and $\mathbf{b}_3$ are reciprocal lattice vectors of GeAs.

	$\times\mathbf{b}_1$	$\times\mathbf{b}_2$	$\times\mathbf{b}_3$
Γ	0.00000	0.00000	0.00000
Y	-0.50000	-0.50000	0.00000
F	-0.55269	-0.55269	0.41235
L	-0.50000	-0.50000	0.50000
I	-0.73788	-0.26212	0.50000
I_1	-0.26212	0.26212	0.50000
Z	0.00000	0.00000	0.50000
F_1	-0.44731	-0.44731	0.58765
X_1	-0.73372	-0.26628	0.00000
X	-0.26628	0.26628	0.00000
N	-0.50000	0.00000	0.00000
M	-0.50000	0.00000	0.50000

References

1. F. Giustino, M. L. Cohen and S. G. Louie, *Phys. Rev. B*, 2007, **76,** 165108.
2. M. Gao, Q.-Z. Li, X.-W. Yan and J. Wang, *Phys. Rev. B*, 2017, **95,** 024505.
3. W. Li, J. Carrete, N. A. Katcho and N. Mingo, *Comput. Phys. Commun.*, 2014, **185**, 1747-1758.